

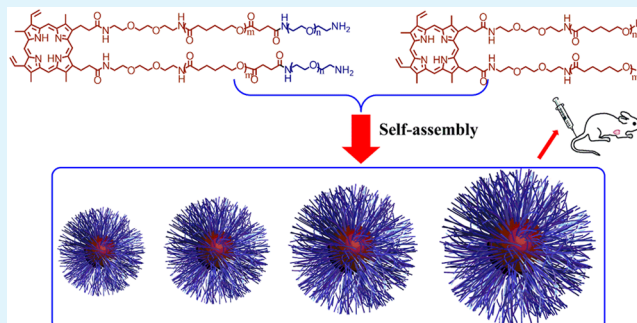
Synthesis and Biological Properties of Porphyrin-Containing Polymeric Micelles with Different Sizes

Jiali Zhang, Zhengkui Zhang, Bo Yu, Chen Wang, Wei Wu,* and Xiqun Jiang*

MOE Key Laboratory of High Performance Polymer Materials and Technology, Department of Polymer Science & Engineering, College of Chemistry & Chemical Engineering, and Jiangsu Key Laboratory for Nanotechnology, Nanjing University, Nanjing, 210093, People's Republic of China

Supporting Information

ABSTRACT: To understand the size effect of polymeric micelles on their biological properties, such as cellular uptake, biodistribution, tumor accumulation, and so on, we prepared a series of doxorubicin (DOX)-loaded protoporphyrin (PP)-poly(ϵ -caprolactone) (PCL)-poly(ethylene glycol) (PEG) micelles with different diameters (40, 70, 100, and 130 nm). The incorporation of the protoporphyrin moiety enhanced the stability of the micelles and provided luminescent capability that is useful in the investigation of the cellular uptake of the micelles by fluorescence imaging. The biodistributions of the micelles in mice bearing tumors were evaluated by near-infrared fluorescence imaging and DOX concentration measurements in different tissues. The in vitro and in vivo investigations demonstrated the pronounced dependence of the cellular uptake, biodistribution, and antitumor effectiveness of the micelles on their size.



KEYWORDS: polymeric micelles, protoporphyrin, size dependence, cellular uptake, biodistribution

1. INTRODUCTION

Nanoscaled polymer micelles have been considered to be very helpful in tumor treatment due to their typical advantages, for example, they can selectively target tumors via the enhanced permeability and retention (EPR) effect and their general physicochemical properties including size, composition, surface chemistry and stability can be adjusted by changing the chemical structures of the amphiphilic copolymers used to prepare polymer micelles in a wide range.^{1–11} Furthermore, these physicochemical properties of the polymer micelles are crucial factors influencing their fates in living systems and their overall drug-delivery properties.^{1,5,10,12–22} Therefore, well-designed polymer micelles have huge potential in the application of tumor treatment.

So far, different types of nanomaterials have been studied to find out the size effect of nanomaterials on their in vivo behaviors,^{9,23–36} such as PEGylated gold nanoparticles,³³ PEGylated silica nanoparticles,³⁴ polymer particles prepared from poly(ethylene glycol)-*b*-poly(glutamic acid) copolymer,³⁵ and so on. However, these different types of nanomaterials have shown different size dependencies of their biodistribution even if they have similar surface chemistry. This indicates that the internal structures of nanomaterials, which influence their deformability, porosity, and so on, may also significantly influence their biological properties. Therefore, more studies are necessary to understand clearly the size dependency of nanomaterial biodistribution and biological properties.

In this study, we prepared protoporphyrin-containing polymer micelles from an amphiphilic block copolymer. This block copolymer consists of protoporphyrin, poly(ethylene glycol) (PEG), and poly(ϵ -caprolactone) (PCL). These components provide the micelles with good biocompatibility, biodegradability and antibiofouling ability. The π – π stacking interactions between the protoporphyrin moieties may enhance the stability of the micelles. By changing the ratio of the components, four types of doxorubicin (DOX)-loaded micelles with diameters of 40, 70, 100, and 130 nm were prepared. The size effects on the cellular uptake, biodistribution and antitumor effectiveness of the drug-loaded micelles were studied. This work may provide a useful guidance for the design of polymer micelles as drug carriers.

2. MATERIALS AND METHODS

2.1. Materials. Protoporphyrin IX (PP), 2,2'-(ethylenedioxy)bis(ethylamine) (TEG), diisopropylcarbodiimide (DIC), ϵ -caprolactone (ϵ -CL), succinic anhydride, poly(ethylene glycol) diamine (PEG, M_n = 2000 Da), NIR-797 isothiocyanate, doxorubicin hydrochloride (DOX-HCl) were bought from Sigma Chemical Co. All other reagents were obtained from commercial suppliers and used without further purification. Murine hepatic tumor cell line H22 was supplied by Shanghai Institute of Cell Biology (Shanghai, China). Male ICR mice

Received: November 11, 2015

Accepted: February 19, 2016

Published: February 19, 2016

were purchased from the Experimental Animal Center of Nanjing Medical University (Nanjing, China).

2.2. Synthesis of PP-(TEG)₂. Protoporphyrin IX (PP) (100 mg, 0.18 mmol) was dissolved in 5 mL of dimethylformamide (DMF). To the solution were added trimethylamine (TEA) (27 μ L, 0.20 mmol) and diisopropylcarbodiimide (30 μ L, 0.20 mmol). The resulting mixture was stirred for half an hour in an ice bath. The reaction mixture was added dropwise to a solution of 2,2'-(ethylenedioxy)bis(ethylamine) (148 μ L, 1.0 mmol) in 5 mL of DMF and the resultant mixture was stirred for 24 h at room temperature. The crude product was purified by column chromatography with an eluent of DCM/methanol = 15:1 to give a dark purple solid (107 mg, 73% yield). ¹H NMR (Figure S1, 300 MHz, DMSO, δ): 2.72 (8H, m), 2.95 (8H, m), 3.05 (10H, m), 3.64 (6H, m), 3.76 (6H, m), 4.34 (4H, t), 6.23 (2H, d), 6.46 (2H, dd), 7.96 (2H, s), 8.45 (2H, dd), 10.25–10.40 (4H, m). C₄₆H₆₂N₈O₆, ESI-MS: *m/z* 823.49 [M + H]⁺.

2.3. Synthesis of PP-PCL. PP-(TEG)₂ (20 mg, 0.036 mmol), stannous octoate (1.00 mg, 2.5 μ mol) and ϵ -caprolactone (0.5 g, 4.4 mmol) were mixed under argon in a 10 mL flask. The resulting mixture was stirred at 130 °C for 48 h under argon. Thereafter, the crude product was purified by precipitating from CH₂Cl₂ to methanol and washing with diethyl ether. After being dried under vacuum, PP-PCL was obtained (300 mg, M_n = 9000 Da). M_n is calculated by comparing the integral intensity of –COCH₂CH₂CH₂CH₂CH₂O– signal at δ = 1.63 with that of –COCH₂CH₂CH₂CH₂CH₂OH at δ = 3.65 in NMR spectra, (Figure S2). ¹H NMR (300 MHz, CDCl₃, δ): 1.37 (166H, m), 1.63 (363H, m), 2.31 (160H, t), 3.65 (4H, t), 4.06 (162H, t).

2.4. Synthesis of PP-PCL-COOH. PP-PCL (200 mg), succinic anhydride (20 mg, 0.20 mmol) and TEA (30 μ L, 0.22 mmol) were dissolved in 5 mL of CH₂Cl₂ and the resulting mixture was stirred at room temperature for 12 h. Thereafter, the crude product was purified by precipitating from CH₂Cl₂ to methanol and washing with diethyl ether. After being dried under vacuum, PP-PCL-COOH was obtained (200 mg). ¹H NMR (Figure S3, 300 MHz, CDCl₃, δ): 1.39 (213H, m), 1.63 (441H, m), 2.30 (206H, t), 2.64 (8H, s), 4.08 (209H, t).

2.5. Synthesis of PP-PCL-PEG. Amine-terminated PEG (400 mg, 0.20 mmol) and PP-PCL-COOH (100 mg, 0.013 mmol) were dissolved in 10 mL of dry CH₂Cl₂. To the resulting solution were added DIC (20 μ L, 0.13 mmol) and TEA (20 μ L, 0.15 mmol). The resultant mixture was stirred for 3 days at room temperature. The crude product was washed with diethyl ether several times and dialyzed against deionized water for 3 days in a 14 kDa MWCO membrane. The obtained suspension was lyophilized to provide a solid PP-PCL-PEG (166 mg, 82%). ¹H NMR (Figure S4, 300 MHz, CDCl₃, δ): 1.38 (129H, m), 1.63 (289H, m), 2.30 (127H, t), 3.38 (4H, s), 3.63 (369H, s), 4.06 (125H, t).

2.6. Synthesis of NIR-797-Labeled PP-PCL-PEG (Scheme S1). PP-PCL-PEG (20 mg, 1.54 \times 10⁻³ mmol) and NIR-797 isothiocyanate (1.0 mg, 1.14 \times 10⁻³ mmol) were dissolved in anhydrous DMF (0.5 mL) containing several drops of TEA and stirred at room temperature for 24 h. The resulting mixture was precipitated in diethyl ether and the obtained precipitate (PP-PCL-PEG-NIR-797) was dialyzed for 24 h against deionized water and lyophilized for use later. All of the above procedures were done under darkness.

2.7. Preparation of PP-PCL-PEG Micelles and DOX-Loaded Micelles. PP-PCL-PEG micelles were prepared by the following procedures. Briefly, 10 mg of a mixture of PP-PCL-PEG and PP-PCL was dissolved in 0.2 mL of acetone/ethanol (1/1, v/v). To the resulting solution was added 60 °C hot deionized water to form micelles. The resulting mixture was dialyzed against water and filtered through a 200 nm single-pore membrane to provide a suspension of the micelles in water. When the ratios of PP-PCL-PEG to PP-PCL are 20:1, 10:1, 5:1, and 3:1, the micelles with diameters 40, 70, 100, and 130 nm are obtained and named micelle 1, micelle 2, micelle 3, and micelle 4, respectively.

NIR-797-labeled micelles were prepared by the same procedures but using a mixture of PP-PCL-PEG-NIR-797, PP-PCL-PEG and PP-PCL to replace PP-PCL-PEG and PP-PCL.

DOX-loaded micelles were prepared by the following procedures. Three mg of DOX-HCl was added into a suspension of PP-PCL-PEG micelles (4 mg/mL, 5 mL) in water, then the pH of the system was adjusted to ~8 by using 0.1 N NaOH aqueous solution. The mixture was stirred for 12 h at room temperature. The resulting mixture was dialyzed for 12 h against deionized water and filtered through a 200 nm single-pore membrane to remove free DOX. DOX-loaded micelles were dissolved in 0.3 M HCl in ethanol/water (7/3, v/v). The DOX concentration in the resulting solution was determined by measuring the absorbance at 480 nm and using a pre-established calibration curve. The drug loading content (DL) and the drug loading efficiency (DE) were calculated by using eqs 1 and 2, respectively:

$$\text{DL (\%)} = \frac{\text{weight of DOX in micelles}}{\text{weight of micelles}} \times 100 \quad (1)$$

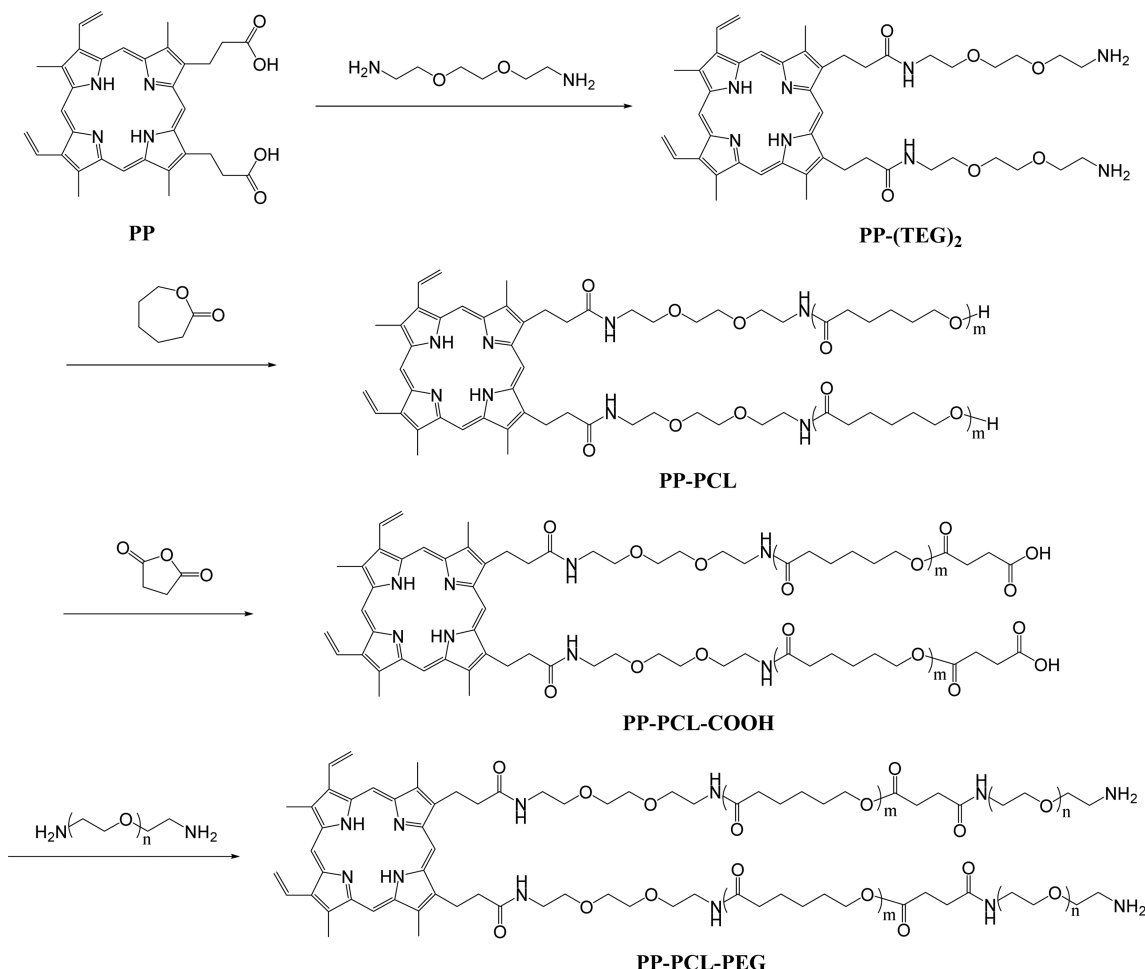
$$\text{DE (\%)} = \frac{\text{weight of DOX in micelles}}{\text{weight of the feeding DOX}} \times 100\% \quad (2)$$

Hydrodynamic diameter of the prepared micelles in water were determined by dynamic light scattering (DLS) on a Brookhaven BI9000AT system (Brookhaven Instruments Corporation, Holtsville, NY). All the measurements were done in triplicate with a wavelength of 658 nm. Before measurements, all the samples were diluted to a predetermined concentration.

DLS was used to assess the stability of the micelles. The suspensions of 4 mg/mL of micelle 1, micelle 2, micelle 3, and micelle 4 in PBS (pH = 7.4, 0.01 mM) were prepared and the hydrodynamic diameter and scattering intensity were examined by DLS at set time points up to 192 h. To examine the stability of the micelles upon dilution, a serial of suspensions of micelle 1, micelle 2, micelle 3, and micelle 4 at concentrations of 4, 2, 1, and 0.5 mg/mL in PBS (pH = 7.4, 0.01 mM) were prepared, and hydrodynamic diameters of the micelles at different concentrations were determined by DLS.

2.8. Determination of Critical Micelle Concentrations (CMCs) of PP-PCL-PEG and PCL-PEG. The CMCs of PP-PCL-PEG and PCL-PEG were determined by using Nile Red as a hydrophobic fluorescence probe.³⁷ The PCL-PEG has similar molecular weight to the PP-PCL-PEG (M_n = 14000 Da) and was synthesized by ring-opening polymerization of ϵ -caprolactone using mPEG (M_n = 5000 Da) as an initiator under the catalysis of stannous octoate. Briefly, mPEG (M_n = 5000 Da, 200 mg), stannous octoate (1.00 mg, 2.5 μ mol) and ϵ -caprolactone (0.5 g, 4.4 mmol) were mixed in a 10 mL flask. The mixture was stirred at 130 °C for 48 h under argon. Thereafter, the crude product was purified by precipitating from CH₂Cl₂ to methanol. After dried under vacuum, PCL-PEG was obtained. And the M_n of PCL-PEG was calculated to be 13000 Da by comparing the integral intensity of –COCH₂CH₂CH₂CH₂CH₂O– signal in PCL at δ = 4.06 with that of –OCH₂CH₂O– in PEG at δ = 3.63 in ¹H NMR spectra of PCL-PEG (Figure S5). A serial of aqueous solutions of PP-PCL-PEG and PCL-PEG with concentrations from 4.0 \times 10⁻⁴, 1.6 \times 10⁻³, 4.0 \times 10⁻³, 4.0 \times 10⁻², 0.16, 0.4 mg/mL containing 6 \times 10⁻⁷ M Nile Red were prepared, respectively. Fluorescence was measured at an excitation wavelength of 560 nm, and the emission was monitored in a range of 580 to 750 nm. Both excitation and emission slit widths were maintained at 5.0 nm, and spectra were acquired with a scan speed of 500 nm/min. The fluorescence intensity at 600 nm was analyzed as a function of the polymer concentration. For the case of PP-PCL-PEG, the fluorescence intensities of PP-PCL-PEG at 600 nm at the set concentrations were measured and subtracted from the corresponding total intensity to exclude the influence of the fluorescence of PP moieties to CMC determination.

2.9. In Vitro Drug Release. In vitro DOX release from the micelles was examined by using a dialysis bag diffusion technique. Predetermined amount of a suspension of DOX-loaded micelles in water was dialyzed against 3 mL of 0.01 M PBS with pH 7.4 and 6.0 respectively at 37 °C with gentle agitation. During the process, 3 mL of the release medium was taken and then the same volume of fresh PBS was replenished periodically. The DOX concentration was determined

Scheme 1. Synthesis of PP-PCL-PEG Block Copolymer

by a fluorescence spectrometer at an excitation wavelength of 480 nm and an emission wavelength of 590 nm.

2.10. In Vitro Cellular Uptake and Cytotoxicity. In vitro cellular uptake and cytotoxicity of DOX-loaded micelles were examined by using murine hepatic carcinoma cell line H22. For cellular uptake, H22 cells were seeded in a 6-well black plate. Then, 200 μL of the suspension of PP-PCL-PEG micelles (4.0 mg/mL) were added to the cultured medium. After incubated at 37 °C for 4 h, the cells were collected by centrifugation, washed three times with PBS. The nucleus was stained with Hoechst 33258 in PBS, and then the cells were checked by confocal laser scanning microscopy (CLSM) at an excitation wavelength of 488 nm.

For quantitative analysis of cell uptake, H22 cells were seeded in a 6-well black plate, and 200 μL of the suspension of PP-PCL-PEG micelles (4.0 mg/mL) were added to the cultured medium. After incubated at 37 °C for 4 h, the cells were collected by centrifugation, washed three times with PBS. Then, the cells were treated by 2 mL of cell lysis solution (150 mM NaCl, 1% Triton X 100, 0.1% SDS, 50 mM Tris pH 8.0) to lyse them. The cellular uptake efficiency was calculated via eq 3.³⁰

$$\text{uptake efficiency (\%)} = \frac{I_{\text{sample}} - I_{\text{negative}}}{I_{\text{positive}} - I_{\text{negative}}} \times 100 \quad (3)$$

The I_{sample} , I_{positive} , and I_{negative} are the fluorescent intensity for the sample, positive control (micelles in cell lysis solution) and negative control (H22 cells without treatment), respectively. The fluorescent intensity was determined at 630 nm with an excitation wavelength of 400 nm.

For in vitro cytotoxicity, the cells were seeded at a density of 10000 cells per well into a 96-well plate and incubated with culture medium

(100 μL) containing different doses of the samples for 48 h at 37 °C. Thereafter, the culture medium was removed and the cells were washed with PBS three times. Then, 20 μL of 3-(4,5-dimethylthiazol-2-yl)-2,5-diphenyltetrazolium bromide (MTT) solution (5 mg/mL) was added to each well, and cultured for another 4 h. After removal of the supernatant, 100 μL of dimethyl sulfoxide (DMSO) was added to each well. The absorbance of each well at 570 nm was measured by an ELISA reader (Huadong, DG-5031, Nanjing).

2.11. Real-Time NIRF Imaging. The real-time near-infrared fluorescence (NIRF) imaging of the H22 tumor-bearing mice after tail-vein injection of the NIR-797-labeled micelles was conducted on a MaestroTM EX fluorescence imaging system (Cambridge Research & Instrumentation, CRi, Woburn, MA). All the animal experiments were approved by Animal Care and Use Committee, Nanjing University. Five $\times 10^6$ murine H22 cells in 0.1 mL of saline were inoculated subcutaneously into the right axillary space of each ICR male mouse. The mice were kept 7 days with free access to water and food. Thereafter, NIR-797-labeled DOX-loaded micelles were injected into H22 tumor bearing mice (25–30 g) via tail vein at a dosage of 4 mg/kg DOX equivalent. The mice were anesthetized with isoflurane and imaged at predetermined time. The NIRF at 845 nm was collected.

2.12. In Vivo Analysis of Biodistribution. DOX-loaded micelles or free DOX in saline were injected via tail vein into H22 tumor-bearing mice at a dose of 4 mg of DOX equivalent per kilogram of body weight. Three mice were included for each time point. At set time intervals, blood were sampled via ophthalmic artery. By centrifuging the blood samples at 4000 rpm for 5 min, plasma was obtained. The mice were killed humanely. Their hearts, livers, spleens, lungs, kidneys, and tumors were harvested and weighed. The plasma and tissues were dispersed in 70% ethanol containing 0.3 M HCl and

Table 1. Hydrodynamic Diameter, Drug Loading Content (DL), and Drug Encapsulation Efficiency (EE) of DOX-Loaded Micelles 1–4

micelle	weight ratio of PP-PCL-PEG to PP-PCL	diameter (nm) ^a	DL (wt %)	EE (%)
1	20:1	44.8 ± 3.2	10.4	69.3
2	10:1	66.7 ± 2.8	11.7	78.0
3	5:1	104.9 ± 6.2	11.3	75.3
4	3:1	131.2 ± 11.0	12.6	84.0

^aHydrodynamic diameter was measured by DLS.

vigorously homogenated. After centrifuging the tissue homogenates thoroughly, the fluorescence intensity of DOX in the supernatant at 590 nm was measured with an excitation wavelength of 480 nm. The DOX concentration in each tissue sample was calculated based on pre-established calibration curves, which were established by adding predetermined amounts of DOX-loaded micelles to the samples of blood or other tissues harvested from untreated mice, followed by the same homogenization and extraction procedures as described above.

2.13. In Vivo Antitumor Efficacy and Survival Rate. An H22 cell suspension (0.1 mL) containing $5-6 \times 10^6$ cells was injected subcutaneously into the right axillary space of the male ICR mice with an average body weight of 25 g. When the tumor volume reached a mean volume of 70–100 mm³, the treatments were started. The day was designated as “day 1”. On day 1, mice were equally randomized into several groups (eight per group). Saline and drug-free micelles were used as control experiments. A dosage of 4 mg/kg DOX equivalent was administered for different DOX formulations. Tumor size was measured every other day, and tumor volume (V) was calculated as $V = W^2 \times L/2$, where W and L are the width and length of the tumor, respectively, and the survival rates were also monitored throughout the experiment.

2.14. Statistical Analysis. Student's *t* test was used to evaluate the difference of antitumor effectiveness between DOX-loaded micelles and free DOX, and *P* values less than 0.05 were considered statistically significant.

3. RESULTS AND DISCUSSION

3.1. Preparation of PP-PCL-PEG Micelles. The synthesis route of the PP-PCL-PEG copolymer is shown in **Scheme 1**. First, PP-(TEG)₂ was synthesized by the amidation reaction between the carboxylic acid groups in protoporphyrin and one of the amino groups in diaminotri(ethylene glycol) by using a large excess of diaminotri(ethylene glycol) as displayed in **Scheme 1**. Thereafter, PP-PCL was synthesized by ring-opening polymerization of ϵ -caprolactone by using PP-(TEG)₂ as an initiator under the catalysis of stannous octoate. The copolymer was purified by precipitating from CH₂Cl₂ to cold methanol several times. After converting the hydroxyl end groups of PP-PCL to carboxylic acid groups by using succinic anhydride, we synthesized PP-PCL-PEG through the reaction between the carboxylic acid groups and one of the amino groups of diaminopoly(ethylene glycol). The number-average molecular weights of PP-PCL and PP-PCL-PEG were determined to be 9000 and 14 000 Da, respectively, using ¹H NMR. Micelles were prepared by adding a certain amount of water to a solution of PP-PCL-PEG and PP-PCL in acetone/ethanol (1/1, v/v) (see **Materials and Methods** for detailed procedures). By changing the ratio of PP-PCL-PEG to PP-PCL to modulate the proportion of hydrophobic components, we can adjust the size of the micelles. When the weight ratios of PP-PCL-PEG to PP-PCL are 20:1, 10:1, 5:1, and 3:1, the micelles with diameters of 40 nm (micelle 1), 70 nm (micelle 2), 100 nm (micelle 3), and 140 nm (micelle 4) determined by DLS can be obtained, respectively. The stability of the micelles upon aging and dilution was studied by DLS. No

significant change was found in hydrodynamic diameter and scattering intensity when the suspensions of 4 mg/mL of micelle 1, micelle 2, micelle 3, and micelle 4 in PBS (pH = 7.4, 0.01 mM) were monitored over 192 h (**Figure S6a,b**); furthermore, when the suspensions of the micelles were diluted from 4 to 0.5 mg/mL, the sizes of the micelles did not change significantly either (**Figure S6c**), indicating the desirable stability of the micelles.

To check if $\pi-\pi$ stacking interactions between the protoporphyrin moieties occur in the micelles, we compared UV-vis spectrum of micelle 1 in deionized water with the spectra of protoporphyrin aqueous solutions with pH 2 and 6, respectively, because it has been demonstrated that protoporphyrin exists as monomer at pH 0–3 and remarkably aggregates in the pH range 3–7 in aqueous solution, and this can be clearly reflected by Soret absorption band.³⁸ As shown in **Figure S7**, a strong Soret absorption band located at 407 nm is found in the absorption spectrum of protoporphyrin at pH 2, by contrast, at pH 6, the Soret band splits in two bands with maxima at 350 and 463 nm. In the spectrum of micelles 1, two weak absorption peaks located at 350 and 463 nm are observable apart from the strongest peak at 407 nm in the range of 300–500 nm, indicating that there are indeed $\pi-\pi$ stacking interactions between the protoporphyrin moieties in the micelles that may enhance the stability of the micelles.

To verify the role of protoporphyrin in enhancing the stability of the micelles, we determined the CMC of PP-PCL-PEG by fluorescence technique with Nile Red as a hydrophobic fluorescent probe and compared with that of PCL-PEG. The amphiphilic copolymers would self-assemble into polymeric micelles when their concentrations exceed CMC, and Nile Red would be simultaneously encapsulated into the micelle's hydrophobic core. This leads to a sharp increase in the fluorescence intensity of Nile Red. The CMC was determined by extrapolating the fluorescence intensity of Nile Red at 600 nm versus concentrations of PP-PCL-PEG and PCL-PEG, respectively. For the case of PP-PCL-PEG, because the PP-PCL-PEG also has fluorescence at 600 nm due to the presence of PP moieties, the fluorescence intensities of PP-PCL-PEG at 600 nm at set concentrations were measured and subtracted from the corresponding total intensity to exclude the influence of the fluorescence of PP moieties to CMC determination. The CMC of PP-PCL-PEG and PCL-PEG is determined to be 2.79×10^{-2} and 3.28×10^{-2} mg/mL, respectively. Because the PP-PCL-PEG and PCL-PEG have similar molecular weight (14000 Da versus 13000 Da) and similar length ratio of PCL to PEG, the slight reduction of CMC of PP-PCL-PEG relative to PCL-PEG should be caused by the $\pi-\pi$ stacking interaction between the protoporphyrin moieties in PP-PCL-PEG, demonstrating that the presence of the protoporphyrin moiety in PP-PCL-PEG can improve the stability of the micelles.

DOX was loaded into the micelles as a model drug by simply stirring the mixture of micelles and DOX at pH 8.0. The drug

loading content (DL) and drug encapsulation efficiency (EE) of DOX-loaded micelles are summarized in Table 1. The drug-free and drug-loaded micelles show no remarkable difference in size. The representative transmission electron microscopy (TEM) images of the DOX-loaded micelles are shown in Figure 1. It is found that all the DOX-loaded micelles are nearly

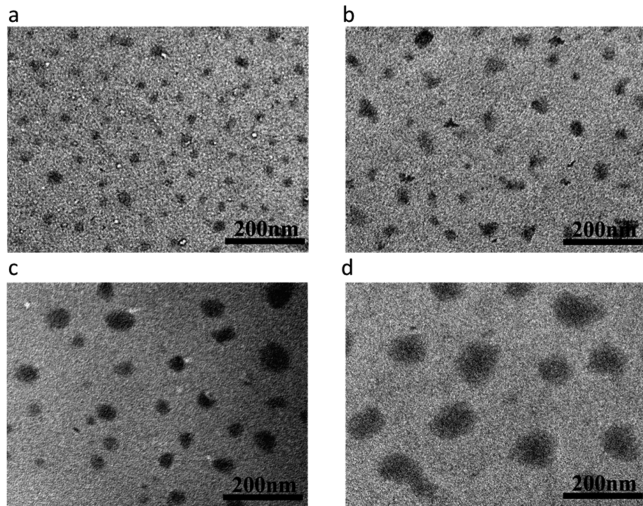


Figure 1. Typical TEM images of DOX-loaded (a) micelle 1, (b) micelle 2, (c) micelle 3, and (d) micelle 4.

spherical in shape with narrowly distributed size. The hydrodynamic diameters of the DOX-loaded micelles were examined by dynamic light scattering (DLS; Table 1) and are obviously larger than the corresponding diameter determined by TEM due to the shrinkage of the micelles in dry state in TEM examinations.

As a drug carrier, the drug loading content and efficiency of the micelles are important parameters for their applications in

tumor treatment. All the four types of PP–PCL–PEG micelles have desirable drug loading content (>10%) and efficiency (>69%; Table 1). Figure 2a,b shows the in vitro drug release profiles of the DOX-loaded micelles in buffer solutions at pH 7.4 and 6.0 at 37 °C, respectively. It is notable that a typically sustained release profile is presented for each of the micelles at both pH 7.4 and 6.0, and the drug release process is significantly accelerated when the medium pH value is reduced from 7.4 to 6.0 because the increased protonation of DOX at lower pH would increase its water solubility. For example, for the four types of drug-loaded micelles, 33–39% of DOX are released within 120 h at pH 7.4, whereas the released portion increases to 70–76% at pH 6.0 in the same period (Figure 2a,b).

3.2. Cytotoxicity and Cellular Uptake. To evaluate the pharmacological activity of the DOX-loaded micelles, the in vitro cytotoxicity of the DOX-loaded/-free micelles against hepatic H22 tumor cells was studied with DOX as a positive control. The cell viability was examined after incubation with a series of doses of DOX formulations and drug-free micelles for 48 h. As shown in Figure 2c, all the drug-free micelles do not show detectable cytotoxicity at all test concentrations, indicating their good cytocompatibility. All the DOX-loaded micelles have comparable cytotoxicity, which is lower than the cytotoxicity of free DOX at a dose larger than 0.5 µg/mL DOX equivalent. This may be caused by the sustained drug release profiles of the DOX-loaded micelles.

The inherent fluorescent characteristic of protoporphyrin moiety in PP–PCL–PEG copolymer can be used to trace the cellular uptake behavior of the micelles by using fluorescence imaging, for example, confocal laser scanning microscopy (CLSM). After incubating H22 cells with the four types of drug-free micelles at 37 °C for 4 h and staining the nucleus with Hoechst 33258, we observed the cells by CLSM. Figure 3 shows the representative CLSM images of the H22 cells incubated with the different micelles. It can be seen that all four

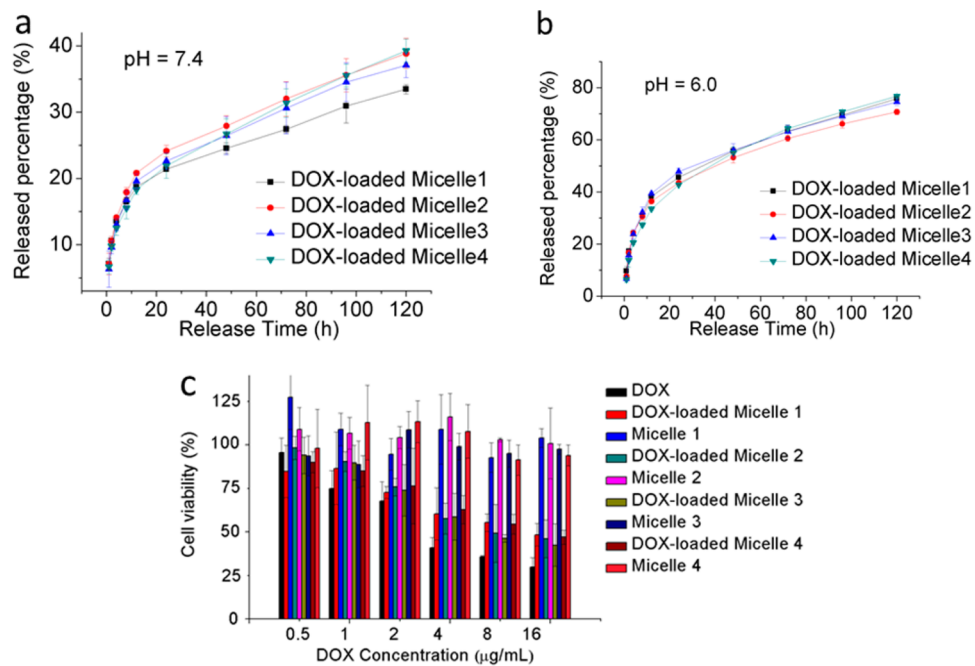


Figure 2. In vitro release profiles of DOX-loaded PP–PCL–PEG micelles in PBS (0.01 M) with a pH of (a) 7.4 and (b) 6.0 at 37 °C. (c) In vitro cytotoxicity of DOX, DOX-free, and DOX-loaded micelles against H22 cell lines after incubation for 48 h.

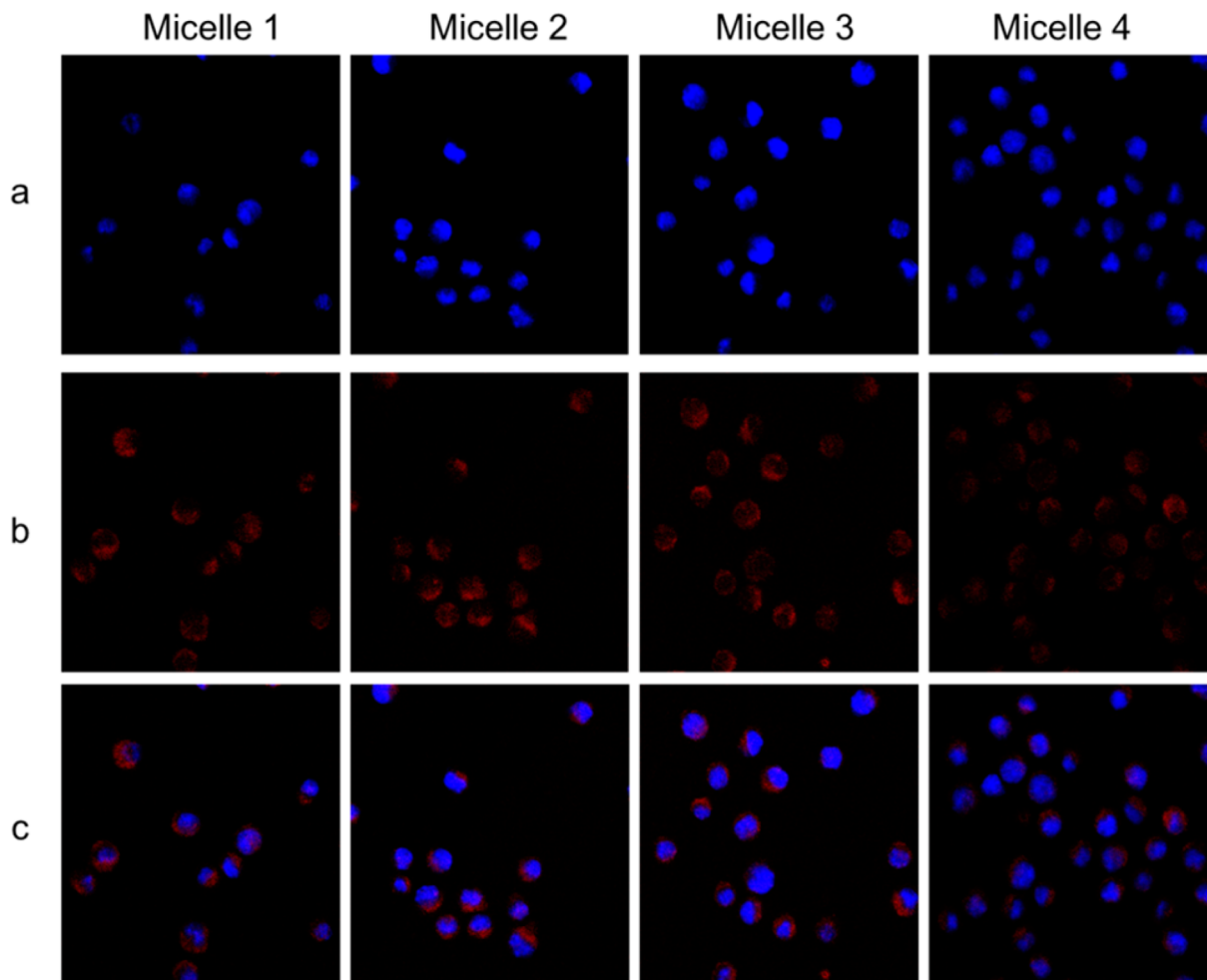


Figure 3. CLSM images of H22 cells incubated with micelle 1–4 at 37 °C for 4 h; (a) blue channel (nucleus), (b) red channel (PP–PCL–PEG micelles), and (c) merged.

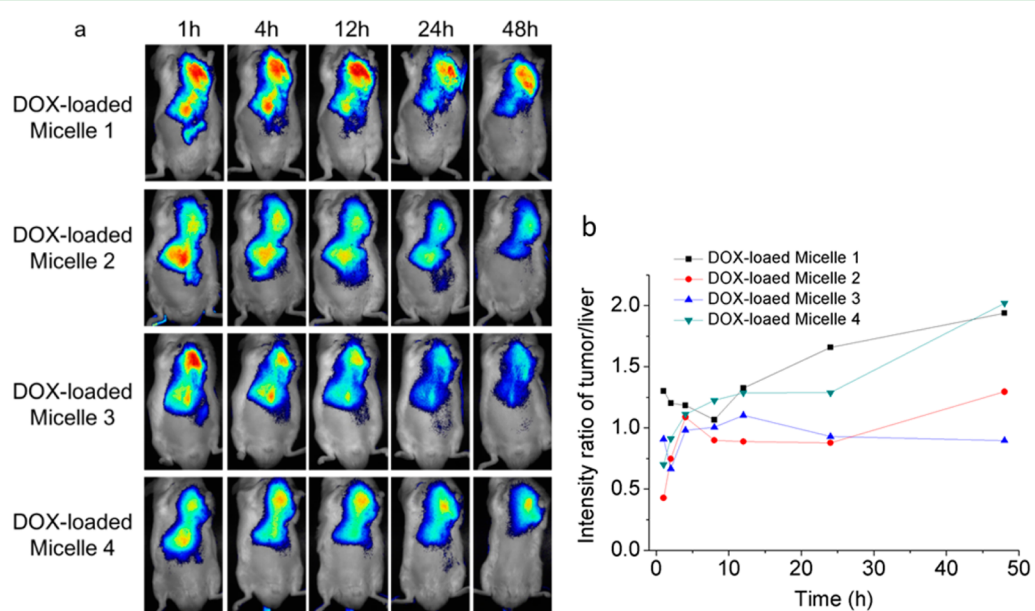


Figure 4. (a) NIFR images of H22 tumor-bearing mice after tail-vein injection of NIR-797-labeled and DOX-loaded micelle 1, micelle 2, micelle 3, and micelle 4, respectively. (b) Average fluorescence intensity ratio of tumor/liver from mice treated with different types of micelles at different time points.

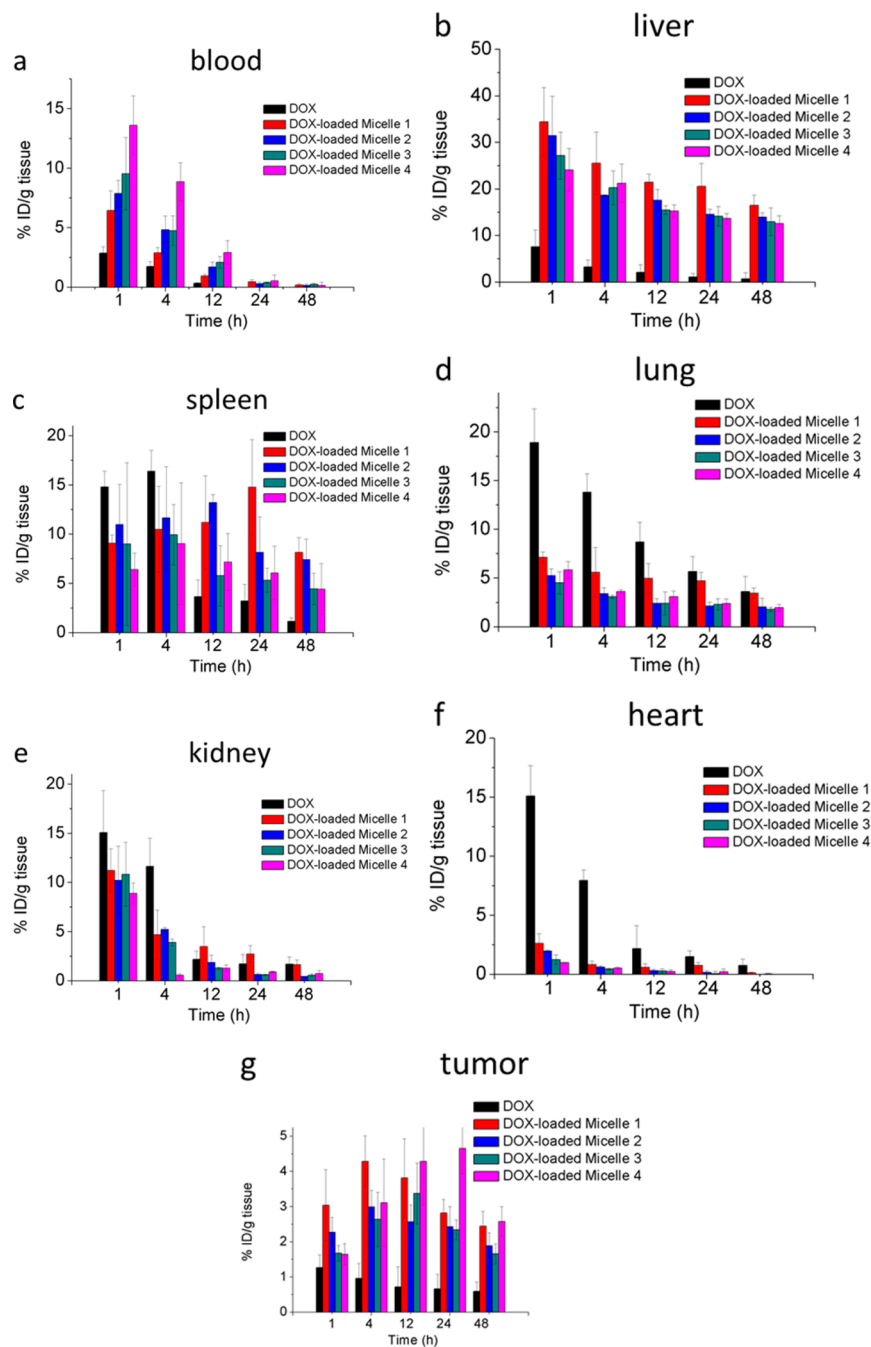


Figure 5. Biodistribution of DOX in different tissues of H22 tumor-bearing mice at different time points after tail-vein injection of free DOX and DOX-loaded micelles 1–4 in (a) blood, (b) liver, (c) spleen, (d) lung, (e) kidney, (f) heart, and (g) tumor. The values are expressed as the percentage of ID per gram of collected tissues and are based on three mice per group.

types of micelles can enter the H22 cells, and few micelles can enter nuclei. To quantitatively compare the cellular uptake of the four types of micelles, the H22 cells incubated with the different drug-free micelles were lysed with cell lysis solution (150 mM NaCl, 1% Triton X 100, 0.1% SDS, 50 mM Tris pH 8.0), and the resulting solutions were analyzed by fluorescent quantitation. The uptake percentage is expressed by the ratio of fluorescence intensity of the incubated H22 cells to that of the micelles in the feeding solution. The uptake percentages for micelles 1–4 are 9.03, 6.67, 4.51, and 4.00%, respectively. The size dependence of cellular uptake is markedly observed, that is to say, the smaller micelles have higher cellular uptake percentage.

3.3. Real-Time NIRF Imaging. The fate of the micelles with different size in tumor-bearing mice was examined first by *in vivo* real-time noninvasive near-infrared fluorescence (NIRF) imaging. Figure 4a shows the typical NIRF fluorescence images of the mice at different time after tail-vein injection of the four types of NIR-797-labeled and DOX-loaded PP-PCL-PEG micelles, respectively. From Figure 4a, it is found that most of the fluorescence signal is in the liver and tumor regions since 1 h postinjection, indicating that all four types of micelles can rapidly accumulate in tumors and as general nanomaterials, they are susceptible to the capture of reticuloendothelial system (RES), leading to the remarkable accumulation in livers. To further understand the tumor targeting ability of the micelles

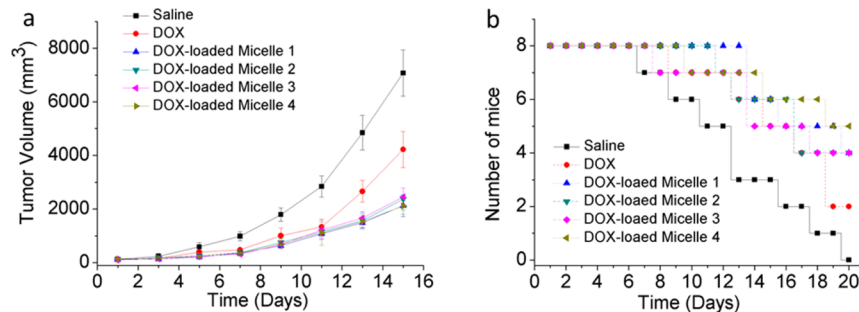


Figure 6. (a) Tumor volume of H22 tumor-bearing mice treated with different micelles and free DOX as indicated. (b) Survival rates of tumor-bearing mice received different treatments as indicated.

with different sizes, we normalized the fluorescence images by using a constant exposure time and compared the signal intensities per unit area in tumor and liver regions (Figure 4b). We can see that for both DOX-loaded micelle 1 and micelle 4, the signal intensity ratios of tumor to liver increase as time elapsed and are larger than that of DOX-loaded micelle 2 or micelle 3 over the monitoring duration especially from 12 h postinjection, indicating the relatively good passive targeting ability of DOX-loaded micelle 1 and micelle 4 to tumors.

3.4. Biodistribution in Vivo. To gain insight into the drug-delivery properties of the micelles with different sizes, we analyzed quantitatively the distribution of DOX in mice bearing tumors as a function of time after injection of the four types of micelles via tail vein, respectively (Figure 5). DOX concentrations were measured by using fluorescence technique after extracting DOX from tissue homogenates. The blood clearance profiles of the micelles are shown in Figure 5a. The elimination half-lives of DOX-loaded micelle 1, micelle 2, micelle 3, micelle 4, and free DOX in blood circulation are calculated to be 2.44, 4.48, 3.31, 4.75, and 0.5 h, respectively. It is notable that all the micelles can prolong the blood circulation time of DOX by encapsulating it inside, and the larger micelles have longer blood circulation time, except for a slight reflection of DOX-loaded micelle 3. It is notable that in liver, lung, and spleen, DOX-loaded micelle 1 provides relatively higher DOX concentrations compared to other micelles at all test time points (Figure 5b–d). These results plus the relatively short blood circulation time of DOX-loaded micelle 1 suggest that such small micelles may be more susceptible to the capture of the RES. The relatively higher DOX concentrations in kidney for the cases of free DOX and DOX-loaded micelle 1 suggest that these two DOX formulations can be eliminated by renal excretion more easily than others (Figure 5e). All the micelle formulations provide similar DOX concentrations in heart, which are much lower than the case of free DOX, indicating that the micelle formulations can reduce the cardiotoxicity toxicity of DOX. Comparing to free DOX, the micelles can transport DOX to tumors much more efficiently. The maximum DOX concentrations in tumors in the monitoring duration for the cases of DOX-loaded micelles 1–4 and free DOX are 4.28% ID/g at 4 h, 2.99% ID/g at 4 h, 3.38% ID/g at 12 h, 4.65% ID/g at 24 h and 1.26% ID/g at 1 h postinjection, respectively. The continuous increase of DOX concentration in tumor tissues for micelle 4 within first 24 h postinjection is consistent with its longer circulation time.

3.5. Antitumor Effect in Vivo. To explore the size effect on the antitumor activities of the micelles, the antitumor properties of the four types of micelles were examined by using subcutaneous H22 tumor-bearing mice as model animals and

compared with that of DOX at a dose of 4 mg of DOX equivalent per kilogram of body weight. The saline-treated group was used as control. When tumor volume reaches $\sim 100 \text{ mm}^3$, the different DOX formulations were injected via tail vein as a solution/suspension in 0.2 mL of saline, respectively. The tumor volumes were measured every other day and are shown in Figure 6a. It is found that the tumors of saline-treated group grow fastest among all the test groups and the average volume reaches $7076.48 \pm 861.65 \text{ mm}^3$ on day 15. The average tumor volume of DOX-treated group is $4221.03 \pm 673.61 \text{ mm}^3$ on day 15. In contrast, the values for the cases of DOX-loaded micelle 1, micelle 2, micelle 3, and micelle 4 are 2121 ± 405 , 2375 ± 412 , 2454 ± 335 , and $2112 \pm 300 \text{ mm}^3$, respectively. On day 15 postinjection, the tumor growth inhibitions (TGI) for the groups treated with DOX-loaded micelle 1, micelle 2, micelle 3 and micelle 4 are calculated to be 70.0%, 66.4%, 65.3 and 70.2%, respectively, versus 40.3% for the DOX-treated group. The results show that DOX-loaded micelles are more efficient than free DOX in tumor suppression, and DOX-loaded micelle 1 and micelle 4 provide better antitumor effectiveness than DOX-loaded micelle 2 and micelle 3. This is well consistent with the results of DOX distributions discussed above.

The antitumor efficiency of the different DOX formulations can also be reflected by the survival rate of the tumor-bearing mice (Figure 6b). All the mice treated with saline died within 20 days postinjection, and only 2 mice survived in the DOX-treated group during this period. By contrast, on day 20 postinjection, there were 4, 4, 4, and 5 surviving mice for DOX-loaded micelle-1-, micelle-2-, micelle-3-, and micelle-4-treated groups, respectively. This further demonstrates that the micelles can significantly improve the antitumor effectiveness of DOX by encapsulating it.

4. CONCLUSION

In this study, we prepared a series of DOX-loaded PP–PCL–PEG micelles with narrowly distributed sizes (40, 70, 100, and 130 nm) to investigate the size effect of the polymeric micelles on their biological behaviors. It was found that the protoporphyrin moiety could enhance the stability of the micelles and provide luminescent capability for the micelles, which enables us to observe cellular uptake of micelles in label-free fashion. The cellular uptake of the micelles showed that the smaller micelles had higher cellular uptake ability. Biodistribution examination indicated that the DOX-loaded micelles in 40 and 130 nm size have higher drug accumulation in tumor. In vivo antitumor efficacy investigation exhibited that DOX-loaded micelles with 40 and 130 nm size have better antitumor effect than the micelles with 70 and 100 nm size and free DOX. These results indicated that the size of drug-loaded polymer

micelles have a pronounced and complicated effect on their cellular uptake, biodistribution, and antitumor activity.

■ ASSOCIATED CONTENT

Supporting Information

The Supporting Information is available free of charge on the ACS Publications website at DOI: [10.1021/acsami.5b10876](https://doi.org/10.1021/acsami.5b10876).

Additional results including ^1H NMR spectra of products, stability of micelles in PBS, UV-vis spectra of micelle, and synthetic route of NIR-797-labeled PP-PCL-PEG. ([PDF](#))

■ AUTHOR INFORMATION

Corresponding Authors

*E-mail: wuwei@nju.edu.cn.

*E-mail: jiangx@nju.edu.cn.

Notes

The authors declare no competing financial interest.

■ ACKNOWLEDGMENTS

This work was supported by the Natural Science Foundation of China (Nos. 21474045, 51273090, and 51422303), the Specialized Research Fund for the Doctoral Program of Higher Education, and the Program for Changjiang Scholars and Innovative Research Team in University.

■ REFERENCES

- (1) Kataoka, K.; Harada, A.; Nagasaki, Y. Block Copolymer Micelles for Drug Delivery: Design, Characterization and Biological Significance. *Adv. Drug Delivery Rev.* **2001**, *47*, 113–131.
- (2) Duncan, R. The Dawning Era of Polymer Therapeutics. *Nat. Rev. Drug Discovery* **2003**, *2*, 347–360.
- (3) Gaucher, G.; Dufresne, M. H.; Sant, V. P.; Kang, N.; Maysinger, D.; Leroux, J. C. Block Copolymer Micelles: Preparation, Characterization and Application in Drug Delivery. *J. Controlled Release* **2005**, *109*, 169–188.
- (4) Nasongkla, N.; Bey, E.; Ren, J.; Ai, H.; Khemtong, C.; Guthi, J. S.; Chin, S. F.; Sherry, A. D.; Boothman, D. A.; Gao, J. Multifunctional Polymeric Micelles as Cancer-Targeted, MRI-Ultrasensitive Drug Delivery Systems. *Nano Lett.* **2006**, *6*, 2427–2430.
- (5) Adams, M. L.; Lavasanifar, A.; Kwon, G. S. Amphiphilic Block Copolymers for Drug Delivery. *J. Pharm. Sci.* **2003**, *92*, 1343–1355.
- (6) Kwon, G. S.; Kataoka, K. Block-copolymer Micelles as Long-circulating Drug Vehicles. *Adv. Drug Delivery Rev.* **1995**, *16*, 295–309.
- (7) Kakizawa, Y.; Kataoka, K. Block Copolymer Micelles for Delivery of Gene and Related Compounds. *Adv. Drug Delivery Rev.* **2002**, *54*, 203–222.
- (8) Kabanov, A. V.; Batrakova, E. V.; Alakhov, V. Y. Pluronic (R) Block Copolymers as Novel Polymer Therapeutics for Drug and Gene Delivery. *J. Controlled Release* **2002**, *82*, 189–212.
- (9) Maeda, H.; Bharate, G. Y.; Daruwalla, J. Polymeric Drugs for Efficient Tumor-targeted Drug Delivery Based on EPR-effect. *Eur. J. Pharm. Biopharm.* **2009**, *71*, 409–419.
- (10) Nishiyama, N.; Kataoka, K. Current state, Achievements, and Future Prospects of Polymeric Micelles as Nanocarriers for Drug and Gene Delivery. *Pharmacol. Ther.* **2006**, *112*, 630–648.
- (11) Blanazs, A.; Armes, S. P.; Ryan, A. J. Self-Assembled Block Copolymer Aggregates: From Micelles to Vesicles and their Biological Applications. *Macromol. Rapid Commun.* **2009**, *30*, 267–277.
- (12) Chan, J. M.; Zhang, L.; Yuet, K. P.; Liao, G.; Rhee, J. W.; Langer, R.; Farokhzad, O. C. PLGA-lecithin-PEG Core-shell Nanoparticles for Controlled Drug Delivery. *Biomaterials* **2009**, *30*, 1627–1634.
- (13) Liggins, R. T.; Burt, H. M. Polyether-polyester Diblock Copolymers for the Preparation of Paclitaxel Loaded Polymeric Micelle Formulations. *Adv. Drug Delivery Rev.* **2002**, *54*, 191–202.
- (14) Cui, F.; Shi, K.; Zhang, L.; Tao, A.; Kawashima, Y. Biodegradable Nanoparticles Loaded with Insulin-phospholipid Complex for Oral Delivery: Preparation, in vitro Characterization and in vivo Evaluation. *J. Controlled Release* **2006**, *114*, 242–250.
- (15) Riley, T.; Stolnik, S.; Heald, C. R.; Xiong, C.; Garnett, M. C.; Illum, L.; Davis, S. S.; Purkiss, S. C.; Barlow, R. J.; Gellert, P. R. Physicochemical Evaluation of Nanoparticles Assembled from Poly(lactic acid)-poly(ethylene glycol) (PLA-PEG) Block Copolymers as Drug Delivery Vehicles. *Langmuir* **2001**, *17*, 3168–3174.
- (16) Bae, Y.; Fukushima, S.; Harada, A.; Kataoka, K. Design of Environment-sensitive Supramolecular Assemblies for Intracellular Drug Delivery: Polymeric Micelles that are Responsive to Intracellular pH Change. *Angew. Chem., Int. Ed.* **2003**, *42*, 4640–4643.
- (17) Xiong, X.; Lavasanifar, A. Traceable Multifunctional Micellar Nanocarriers for Cancer-targeted Co-delivery of MDR-1 siRNA and Doxorubicin. *ACS Nano* **2011**, *5*, 5202–5213.
- (18) Sakuma, S.; Hayashi, M.; Akashi, M. Design of Nanoparticles Composed of Graft Copolymers for Oral Peptide Delivery. *Adv. Drug Delivery Rev.* **2001**, *47*, 21–37.
- (19) Tachikawa, S.; El-Zaria, M. E.; Inomata, R.; Sato, S.; Nakamura, H. Synthesis of Protoporphyrin-lipids and Biological Evaluation of Micelles and Liposomes. *Bioorg. Med. Chem.* **2014**, *22*, 4745–4751.
- (20) Tsukigawa, K.; Nakamura, H.; Fang, J.; Otagiri, M.; Maeda, H. Effect of Different Chemical Bonds in Pegylation of Zinc Protoporphyrin that affects Drug Release, Intracellular Uptake, and Therapeutic Effect in the Tumor. *Eur. J. Pharm. Biopharm.* **2014**, *89*, 259–270.
- (21) Nakamura, H.; Liao, L.; Hitaka, Y.; Tsukigawa, K.; Subr, V.; Fang, J.; Ulbrich, K.; Maeda, H. Micelles of Zinc Protoporphyrin Conjugated to N-(2-hydroxypropyl)methacrylamide (HPMA) Copolymer for Imaging and Light-induced Antitumor Effects in vivo. *J. Controlled Release* **2013**, *165*, 191–198.
- (22) Rouhani, H.; Sepehri, N.; Montazeri, H.; Khoshayand, M. R.; Ghahremani, M. H.; Ostad, S. N.; Atyabi, F.; Dinarvand, R. Zinc Protoporphyrin Polymeric Nanoparticles: Potent Heme Oxygenase Inhibitor for Cancer Therapy. *Pharm. Res.* **2014**, *31*, 2124–2139.
- (23) Guo, X.; Wei, X.; Jing, Y.; Zhou, S. Size Changeable Nanocarriers with Nuclear Targeting for Effectively Overcoming Multidrug Resistance in Cancer Therapy. *Adv. Mater.* **2015**, *27*, 6450–6456.
- (24) Li, L.; Sun, W.; Zhong, J.; Yang, Q.; Zhu, X.; Zhou, Z.; Zhang, Z.; Huang, Y. Multistage Nanovehicle Delivery System Based on Stepwise Size Reduction and Charge Reversal for Programmed Nuclear Targeting of Systemically Administered Anticancer Drugs. *Adv. Funct. Mater.* **2015**, *25*, 4101–4113.
- (25) Cabral, H.; Makino, J.; Matsumoto, Y.; Mi, P.; Wu, H.; Nomoto, T.; Toh, K.; Yamada, N.; Higuchi, Y.; Konishi, S. Systemic Targeting of Lymph Node Metastasis through the Blood Vascular System by Using Size-Controlled Nano carriers. *ACS Nano* **2015**, *9*, 4957–4967.
- (26) Cabral, H.; Matsumoto, Y.; Mizuno, K.; Chen, Q.; Murakami, M.; Kimura, M.; Terada, Y.; Kano, M. R.; Miyazono, K.; Uesaka, M.; Nishiyama, N.; Kataoka, K. Accumulation of Sub-100 nm Polymeric Micelles in Poorly Permeable Tumours Depends on Size. *Nat. Nanotechnol.* **2011**, *6*, 815–823.
- (27) Song, H.; Rioux, R. M.; Hoefelmeyer, J. D.; Komor, R.; Niesz, K.; Grass, M.; Yang, P.; Somorjai, G. A. Hydrothermal Growth of Mesoporous SBA-15 Silica in the Presence of PVP-stabilized Pt Nanoparticles: Synthesis, Characterization, and Catalytic Properties. *J. Am. Chem. Soc.* **2006**, *128*, 3027–3037.
- (28) Antonietti, M.; Heinz, S.; Schmidt, M.; Rosenauer, C. Determination of the Micelle Architecture of Polystyrene Poly(4-vinylpyridine) Block-copolymers in Dilute-solution. *Macromolecules* **1994**, *27*, 3276–3281.
- (29) Tromsdorf, U. I.; Bigall, N. C.; Kaul, M. G.; Bruns, O. T.; Nikolic, M. S.; Mollwitz, B.; Sperling, R. A.; Reimer, R.; Hohenberg, H.; Parak, W. J.; Forster, S.; Beisiegel, U.; Adam, G.; Weller, H. Size

and Surface Effects on the MRI Relaxivity of Manganese Ferrite Nanoparticle Contrast Agents. *Nano Lett.* **2007**, *7*, 2422–2427.

(30) Sakai, T.; Alexandridis, P. Mechanism of Gold Metal Ion Reduction, Nanoparticle Growth and Size Control in Aqueous Amphiphilic Block Copolymer Solutions at Ambient Conditions. *J. Phys. Chem. B* **2005**, *109*, 7766–7777.

(31) Yasugi, K.; Nakamura, T.; Nagasaki, Y.; Kato, M.; Kataoka, K. Sugar-installed Polymer Micelles: Synthesis and Micellization of Poly(ethylene glycol)-poly(D,L-lactide) Block Copolymers Having Sugar Groups at the PEG Chain End. *Macromolecules* **1999**, *32*, 8024–8032.

(32) Prabaharan, M.; Grailer, J. J.; Pilla, S.; Steeber, D. A.; Gong, S. Amphiphilic Multi-arm-block Copolymer Conjugated with Doxorubicin via pH-sensitive Hydrazone Bond for Tumor-targeted Drug Delivery. *Biomaterials* **2009**, *30*, 5757–5766.

(33) Perrault, S. D.; Walkey, C.; Jennings, T.; Fischer, H. C.; Chan, W. C. W. Mediating Tumor Targeting Efficiency of Nanoparticles through Design. *Nano Lett.* **2009**, *9*, 1909–1915.

(34) Tang, L.; Fan, T. M.; Borst, L. B.; Cheng, J. Synthesis and Biological Response of Size-specific, Monodisperse Drug-silica Nanoconjugates. *ACS Nano* **2012**, *6*, 3954–3966.

(35) Cabral, H.; Nishiyama, N.; Kataoka, K. Optimization of (1,2-diamino-cyclohexane)platinum(II)-loaded Polymeric Micelles Directed to Improved Tumor Targeting and Enhanced Antitumor Activity. *J. Controlled Release* **2007**, *121*, 146–155.

(36) Yin, Q.; Tong, R.; Xu, Y.; Baek, K.; Dobrucki, L. W.; Fan, T. M.; Cheng, J. Drug-initiated Ring-opening Polymerization of O-carboxyanhydrides for the Preparation of Anticancer Drug-poly(O-carboxyanhydride) Nanoconjugates. *Biomacromolecules* **2013**, *14*, 920–929.

(37) Xiao, K.; Li, Y.; Luo, J.; Lee, J. S.; Xiao, W.; Gonik, A. M.; Agarwal, R. G.; Lam, K. S. The Effect of Surface Charge on in vivo Biodistribution of PEG-oligocholic Acid Based Micellar Nanoparticles. *Biomaterials* **2011**, *32*, 3435–3446.

(38) Scolaro, L. M.; Castriciano, M.; Romeo, A.; Patane, S.; Cefali, E.; Allegrini, M. Aggregation behavior of protoporphyrin IX in aqueous solutions: Clear evidence of vesicle formation. *J. Phys. Chem. B* **2002**, *106*, 2453–2459.